10-3-2011

Electrostatically Tunable Meta-Atoms Integrated With In Situ Fabricated MEMS Cantilever Beam Arrays

Ronald A. Coutu Jr.
Marquette University, ronald.coutu@marquette.edu

Peter J. Collins
Air Force Institute of Technology

Elizabeth A. Moore
Wyle Labs

Derrick Langley
Air Force Institute of Technology

Matthew E. Jussaume
Air Force Research Laboratory

See next page for additional authors

Accepted version. *Journal of Microelectromechanical Systems,* Vol. 20, No. 6 (December 2011): 1366 - 1371. DOI.
Ronald A. Coutu was affiliated with the Air Force Institute of Technology, Wright-Patterson Air Force Base, Dayton, OH at the time of publication.

Journal of Microelectromechanical Systems, Vol. 20, No. 6, (December, 2011): 1366-1371. DOI.

Contents

Electrostatically Tunable Meta-Atoms Integrated with In Situ Fabricated MEMS Cantilever Beam Arrays

Ronald A. Coutu
Air Force Institute of Technology, Wright-Patterson Air Force Base, OH
Peter J. Collins
Air Force Institute of Technology, Wright-Patterson Air Force Base, OH
Elizabeth A. Moore
Wyle Labs, Beavercreek, OH
Derrick Langley
Air Force Institute of Technology, Wright-Patterson Air Force Base, OH
Matthew E. Jussaume
Air Force Research Laboratory, Wright-Patterson Air Force Base, OH
Lavern A. Starman
Air Force Institute of Technology, Wright-Patterson Air Force Base, OH

Abstract:

Two concentric split ring resonators (SRRs) or meta-atoms designed to have a resonant frequency of 14 GHz are integrated with microelectromechanical systems cantilever arrays to enable electrostatic tuning of the resonant frequency. The entire structure was fabricated monolithically to improve scalability and minimize losses from externally wire-bonded components. A cantilever array was fabricated in the gap of both the inner and outer SRRs and consisted of five evenly spaced beams with lengths ranging from 300 to 400 µm. The cantilevers pulled in between 15 and 24 V depending on the beam geometry. Each pulled-in beam increased the SRR gap capacitance resulting in an overall 1-GHz shift of the measured meta-atom resonant frequency.

SECTION I. Introduction

Split RING resonators (SRRs) or meta-atoms have received considerable interest over the past decade due to their unique material properties (i.e., effective negative permeability).[1] The SRR, proposed by Pendry et al.,[2] has become the starting point for many metamaterial designs.[3–4,5,6,8–9,10] The SRR structure, however, has a fixed resonant frequency. The resonance is governed by the geometry of the structure and is dependent on the self-inductance of the metal trace and the capacitance from the gap region of the resonator. The resonance mechanism limits the spectral range over which the structure will exhibit negative permeability values. Therefore, determining methods to overcome the static nature of the SRR structure has become a priority in metamaterial research focused on wider bandwidth applications.

The split ring is a resonant particle with a fixed frequency approximately equal to $\omega_0 \approx (L \cdot C)^{-1/2}$, where L is the self-inductance of the metal trace and C is the capacitance of the meta-atom. The capacitance of the meta-atom has contributions from the SRR gap, the gap formed from the inner and outer ring separation, and the interaction from neighboring SRRs.

The most convenient method to tune the resonant frequency of an SRR is to alter the gap capacitance of the split ring. This has been accomplished through the addition of varactor diodes to the structure,[3,4] creating microsplit SRR structures,[5] and loading the SRR with externally wired macrosized capacitors.[6] Liquid crystals have also been employed to dynamically shift the resonant frequency based on their success in tuning the band gaps of photonic crystals.[7] Incorporating externally connected microelectromechanical systems (MEMS) devices into the meta-atom structure has also been investigated.[8,9] Our contribution consists of micromachining SRRs with cantilever beam arrays in the gap region to vary the capacitance and, thus, tune the resonant frequency. This novel approach capitalizes on *in situ* device fabrication, uses less surface area than previous approaches, and does not require externally wire-bonded components (e.g., commercial MEMS switches, varactor diodes, etc.), therefore eliminating associated radiation losses. Additionally, this unique approach provides resonant frequency scalability and improved manufacturability because the SRRs and the MEMS tuning elements are fabricated at the same time.

SECTION II. Design

SRR geometries demonstrated by Smith et al.[10] were chosen as a template to create two generic concentric split rings. The SRR design was modified slightly to create an area large enough for the MEMS cantilever array. The SRR geometry modifications and the cantilever placement shifted the resonance from the 9 GHz of Smith's original design to approximately 14 GHz. The resulting SRR structures, shown in Fig. 1, have a rectangular shape with a height of 2400 μm and a length of 2200 μm. The width of the metal trace is 200 μm, except for the side of the SRR containing the gap which is 400 μm to accommodate the cantilever array. The inner/outer ring separation is 150 μm. The SRR gap separation is 300 μm; however, it has been narrowed in a stair-step fashion (as shown in Fig. 1) to create identical landing pads for each of the cantilever beam capacitors. The stair-step design allows for each cantilever beam to overlap the SRR by the same amount, thus creating an identical capacitor as the previous beam. The landing pad sizing ensures that each capacitor has the same area and thus contributes the same amount to the overall capacitance. The bias lines for the applied actuation voltage and ground lines run alongside the SRRs and have attachment points to the drive electrodes under the cantilevers. Fig. 1 also shows where two approximately 5-μm -wide focused ion beam (FIB) cuts were needed to correct a short that occurred during fabrication.

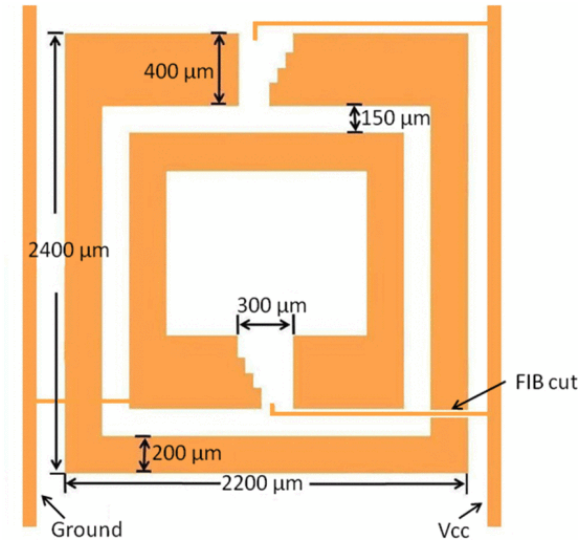

Fig. 1. Schematic diagram of the concentric SRR unit cell showing the stair-step modifications to the SRR gap region and the ground/Vcc bias lines.

The cantilever array, shown in Fig. 2, is composed of cantilever beams that are 75 μm wide and have lengths of 300-, 325-, 350-, 375-, and 400-μm. Each cantilever is anchored at one end of the SRR gap and extends across the gap overlapping the edge of the SRR by 120 μm. The landing area and drive electrodes for the beams are coated with a thin silicon nitride layer to increase the SRR capacitance and avoid beam shorting after pull-in.

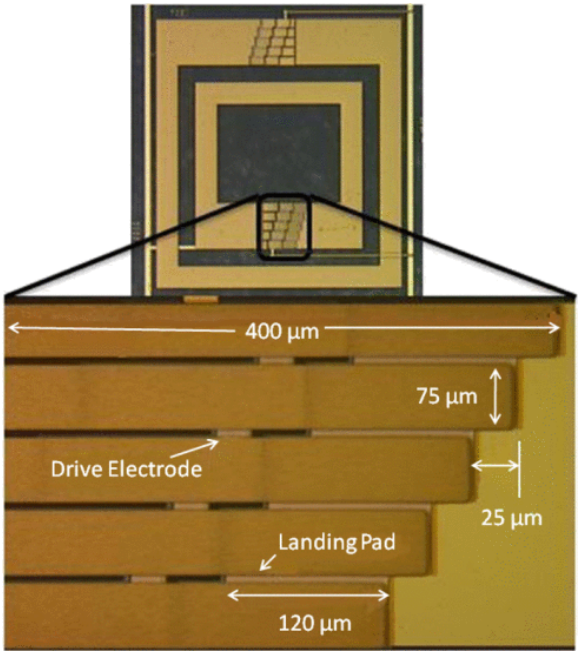

Fig. 2. Image of the SRR showing the cantilever beam array in the gap regions of both the inner and outer SRRs. The cantilever array is enlarged to clearly show the dimensions.

Each beam is electrostatically actuated by applying a dc voltage between the drive electrode and the cantilever. The pull-in voltage for each cantilever, as shown in (1), is dependent on the following: the initial gap height g_0 (2

μm), the dielectric relative permittivity ε_{Si3N4}, the thickness of the dielectric t_d (0.3 μm), the spring constant of the cantilever *k*, and the area of the parallel plate capacitor at the drive electrode *A* (75 μm×120 μm)

(1)

$$V_{\mathrm{pi}} = \frac{2}{3}(g_0 + \frac{\varepsilon_{\mathrm{air}}}{\varepsilon_{\mathrm{Si_3N_4}}} t_d)[\frac{2k}{3\varepsilon_0 A}(g_0 + \frac{\varepsilon_{\mathrm{air}}}{\varepsilon_{\mathrm{Si_3N_4}}} t_d)]^{1/2}.$$

The spring constant was calculated with (2)

(2)

$$k = \frac{E' w t_b^3}{2a^2(3L - a)}$$

where E' is the biaxial modulus (Young's modulus weighted by Poisson's ratio) for electroplated gold, w is the width of the beam, t_b is the thickness of the beam (4.75 μm), *a* is the position on the beam where the electrostatic force is applied, and L is the length of the beam. The spring constants for the 300-, 325-, 350-, 375-, and 400-μm beams were calculated to be 34.7, 20.3, 13.8, 9.8, and 7.3 μN/m, respectively. The model does not account for fringing fields nor the partial deflections of the “next up” beams prior to pull-in. The theoretical pull-in voltages for the 300-, 325-, 350-, 375-, and 400-μm beams are 27.6, 23.5, 20.3, 17.7, and 15.5 V, respectively. The beam length and the spring constant have a reciprocal relationship such that the longest beams pull in first.

With all the beams raised, the gap capacitance is modeled as two capacitors in series. The first capacitor has a separation distance equal to 2 μm, the raised height of the cantilever beams, while the second capacitor has a separation distance equal to the thickness of the dielectric layer, i.e., 0.3 μm. As the beams pull in, they no longer behave as two capacitors in series but rather one capacitor with a separation equal to the thickness of the dielectric. The capacitance due to each beam adds to the capacitance from the other beams to determine the total added capacitance of the MEMS cantilever beam array.

The first actuated beam contributes about 2.07 pF, while the remaining four raised beams still modeled as two capacitors in series will add approximately 0.15 pF. As each beam is actuated, the additional capacitance to the SRR is approximately 2.2, 4.3, 6.3, 8.3, and 10.4 pF as the 400-, 375-, 350-, 325-, and 300- μm beams are pulled-in, respectively.

SECTION III. Fabrication

The fabrication process used to create the tunable SRRs is annotated in Fig. 3, with a picture of the released cantilever array shown in Fig. 4. The structure is built on a 0.5-mm-thick 3-in diameter R-plane highly resistive quartz substrate. First, a base SRR layer is produced by evaporating 5500 rmAA of gold onto a 200-rmAA titanium adhesion layer, shown in Fig. 3(a). Then, a 5500-rmAA -thick gold electrode was deposited onto a 200-rmAA titanium adhesion layer [Fig. 3(b)], followed by [Fig. 3(c)] a 3000-rmAA layer of Si_3N_4 deposited using plasma-enhanced chemical vapor deposition (PECVD). The nitride layer is patterned and then etched with reactive ion etching. Following the removal of the unwanted nitride, polydimethylglutarimide (PMGI) is deposited to form the 2-μm -thick beam gap [Fig. 3(d)]. Next, the anchor area was patterned using SF11, a deep UV photoresist [Fig. 3(e)], followed by a 270 °C hot

plate bake to reflow the hinges [Fig. 3(f)]. The structural layer is formed by dc sputtering a thin layer of gold to form a seed layer [Fig. 3(g)] and then electroplating approximately 5 μm of gold [Fig. 3(h)]. Finally, the PMGI sacrificial layer is removed with 1165 stripper which releases the cantilevers. The sample is then dried in a CO_2 critical point dryer. The completed wafers are inspected and diced into strips containing one row of 17 SRRs with bond pads at one end of the array.

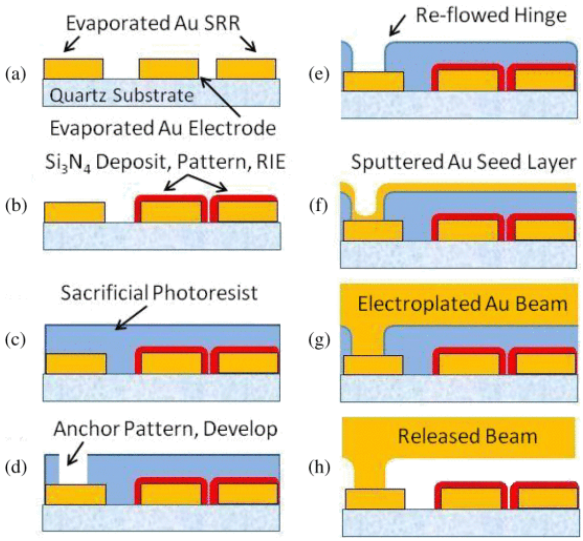

Fig. 3. Annotated fabrication process used to produce the SRRs with the MEMS cantilever beam array in the gap regions.

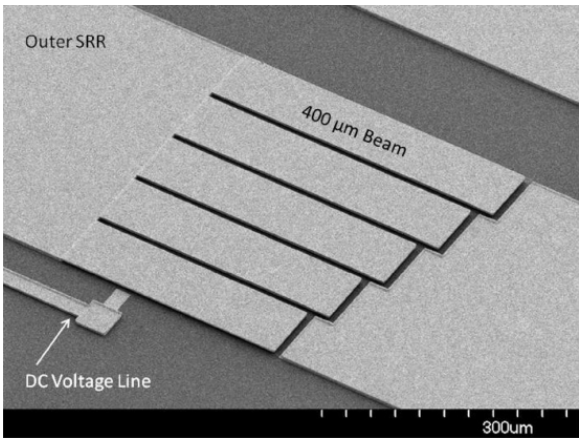

Fig. 4. SEM image showing a released set of cantilever beams across the gap of the outer SRR. Also shown is the dc bias line that connects to the electrodes beneath the beams.

Fig. 4 is a scanning electron microscope (SEM) image of the released cantilever beams on the outer SRR. The image also shows the dc voltage line that connects to the drive electrode beneath the beams. Electroplated film thickness and gap height are measured with a profilometer during fabrication to test for variations in the process. The SRR thickness and gap were found to be uniform across the 1 × 17 array, with a final beam thickness of 4.75 μm and gap height of 2 μm. In addition, the cantilever beams are relatively “flat” not “curled” which is indicative of having low residual stress in the structural layer.

During initial device testing, it was discovered that the Vcc bias line, needed to actuate the inner cantilevers, was shorted to the outer ring. The short was eliminated by using a FIB to mill out the sections of the SRR that came into contact with the Vcc trace. The location of the FIB cut is identified in Fig. 1. The FIB cut removed the short in the Vcc bias line; however, it also disconnected the outer cantilevers from the ground line such that they could no longer be electrostatically actuated. The ground bias line did not require FIB cutting because both rings of the SRRs were intentionally grounded as part of the design.

SECTION IV. Simulations

In an effort to better understand the electromagnetic subtleties in the structure's operation, the SRR/cantilever array was modeled with CST Microwave Studio (CST MWS), a simulation tool for analyzing high-frequency devices.[11] The SRRs were modeled as infinitely thin gold surfaces on a dielectric substrate with ε_r equal to 3.8 to simulate quartz. The inner and outer SRRs were modeled with their gaps in opposite directions, and lumped capacitive elements were used to represent the cantilevers in the gap regions. The capacitance of the outer SRR was held constant at 0.2 pF, the value calculated for when all of the beams are in the raised position. The capacitive values for the cantilever array on the inner SRR were varied from 2.2 to 10.4 pF to simulate the actuation of each of the five beams. Additionally, two 5-μm slits were added to the outer SRR to represent the added parasitic capacitance resulting from FIB cutting around the Vcc voltage line.

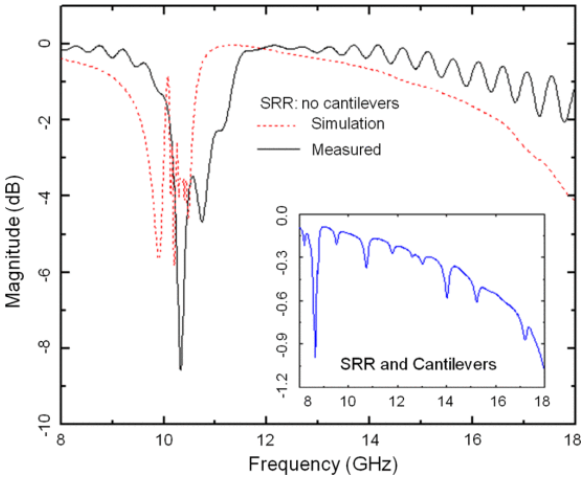

Fig. 5. (Dotted line) Simulated and (solid line) measured results showing a resonance around 10 GHz of the SRRs with no cantilever array in the gap region. The inset shows the simulated transmission of the SRRs with lumped capacitive elements added to represent the cantilever arrays with all the beams in the raised position.

To verify the effectiveness of the CST MWS models, SRRs with no cantilevers were modeled first. The results, along with the measured data from the SRR structures, are shown in Fig. 5. The figure shows the simulation data (dashed line) overlaid with the measured data (solid line) for the concentric SRRs without the MEMS cantilever arrays. The CST simulations of the SRR sans cantilever arrays indicate that a double resonance occurs at 9.9 and 10.3 GHz. The measured data have the dual resonances, as predicted by the simulations, and only the resonance peaks are shifted 0.4 GHz toward higher frequencies. The resonances in the measured data occur at 10.3 and 10.7 GHz. The disagreement observed between the simulations and the measured data for the baseline SRR structures (without

tuning) is not seen once the cantilever arrays have been incorporated, indicating the inherent gap capacitance in the model using infinitely thin metal traces differed from the physical device.

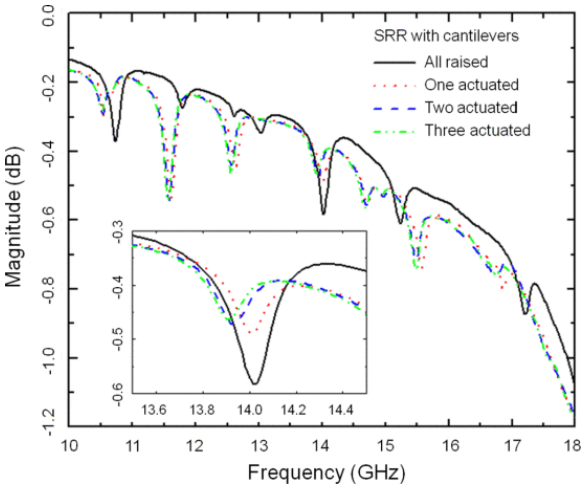

Fig. 6. Simulated transmission for a 1 × 17 array of SRRs with lumped capacitive elements representing the cantilever array. The inset highlights the region around 14 GHz to enhance the tuning behavior of the resonant frequency.

The cantilever beams are modeled in the CST MWS simulations as simple lumped capacitive elements. This simplification will undoubtedly introduce discrepancies between the simulated and measured data. The inset of Fig. 5 shows the simulation data for the SRRs with lumped capacitive elements in the gap regions representing the cantilever array with all the beams in the raised position on both the inner and outer SRRs. The simulations predict that the added capacitance in the gap region produces multiple resonances in the transmission signal, as well as significantly reduces the magnitude of the transmission.

CST MWS simulations of SRRs with varying capacitive elements representing the actuation of the cantilevers are shown in Fig. 6. The simulations indicate that the additional capacitance causes a series of nulls to form that tune slightly toward lower frequencies as the lumped capacitive elements are increased from 2.2 to 6.3 pF. In the inset of Fig. 6, the resonance at 14.02 GHz is enlarged to highlight the effects that the increased capacitance has on the signal. As the capacitance is increased to 2.2 pF to simulate the actuation of the first cantilever, the null does not change frequency, but the magnitude decreases. Further increasing the capacitance to 4.3 pF to simulate the actuation of the second cantilever shifts the resonant frequency by 0.08 GHz to 13.94 GHz. The frequency further shifts to 13.92 GHz as the capacitance is brought up to 6.3 pF to represent the actuation of the third cantilever beam.

The simulation predicts a 0.1-GHz shift in the 14-GHz resonant frequency band using the calculated dc capacitances. The measured data, however, do not have multiple resonant frequencies as indicated by the simulations but rather have one resonance at 14.65 GHz that tunes with the capacitance. This is most likely due to the losses and small alignment variations in the measurement not modeled in the simulations. The result is to detune or reduce the Q of all but the strongest resonances.

SECTION V. Measurements

The fabricated devices were first tested using dc to ensure that the cantilevers functioned as designed. This was followed by RF testing to demonstrate the tuning functionality of the cantilever array design.

The dc testing to verify the beam pull-in voltages was accomplished optically. The pull-in voltages were measured by viewing the cantilevers while increasing the applied voltage until a cantilever beam snapped down, at which point the voltage was recorded. For this measurement, the actuation voltage was applied to individual cantilever beam arrays to measure the pull-in voltages for a single cantilever element. Measured pull-in voltages (during RF testing) for the 300-, 325-, 350-, 375-, and 400-μm beams are 22, 21, 20, 18, and 15 V, respectively. The measured pull-in voltages are repeatable and in good agreement with the voltages calculated with (1), as shown in Table I. The longer beams (300-, 325-, 350-, 375-, and 400-μm) pull in at the calculated voltage, while the shorter beams pull in at voltages slightly less than the calculated pull-in voltages. Differences between the measured voltage and analytic calculations are most likely due to differences in the actual geometries and the thin-film properties of the as-fabricated devices.

Table I Calculated and Measured Pull-In Voltages for a Single Cantilever Array and Measured Pull-In and Pull-Off Voltages for the Entire 1 ×17 SRR Array

Cantilever Length (μm)	Calculated V_{pi} (V)	Measured V_{pi} (V) (one element)	Measured V_{pi} (V) (array)	Measured V_{po} (V) (array)
300	27.6	22	60	12
325	23.5	21	55	10
350	20.3	20	45	8
375	17.7	18	35	6
400	15.5	15	30	4

Table I also lists the measured pull-in and pull-off voltages V_{po} for the entire 1 × 17 array of SRRs. The pulled-in cantilever beams released or pulled off at 12, 10, 8, 6, and 4 V for the 300-, 325-, 350-, 375-, and 400-μm beams, respectively. Minimal pull-in and pull-off voltage variation was observed between the SRR array elements. The pull-in voltages for the entire 1 × 17 SRR array, however, are higher than the pull-in voltages for individual elements of the SRR array. This increased pull-in voltage when actuating the entire 17 element SRR array is indicative of a leakage current or short circuit. To identify the cause of the increased pull-in voltage, thermal images were collected using an OptoTherm thermal imaging system. Fig. 7 is a thermal image of the SRR indicating that the location of the short is near the FIB cut on the first SRR in the array. This location coincides with the attempt to isolate the SRR from the Vcc bias line for the cantilevers. This area of the split ring milled out during FIB cutting successfully isolated the trace and allowed individual element actuation. However, the residue left behind during the FIB process also formed a buried resistive channel sufficient to drop the difference in voltage between the V_{pi} (array) and V_{pi} (one element).

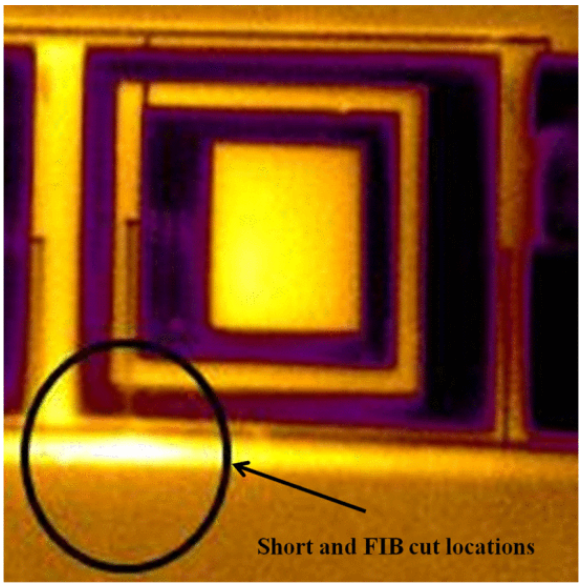

Fig. 7. Thermal image identifying the location of the short and corresponding FIB cuts made to isolate the SRR from the Vcc bias line.

Following dc testing, the meta-atom array was placed in a microwave strip line fixture to measure the S -parameters of the entire structure. The measured RF data of the SRR with MEMS cantilever array are shown in Fig. 8. The measured data have only one resonance centered at 14.65 GHz that tunes to lower frequencies as the capacitance is increased. The resonant frequency of the SRR shifts as the applied voltage is increased from 0 to 40 V, in 20 V increments. The addition of the cantilever array causes a significant reduction in transmission frequency when compared to the SRRs sans cantilever beam array (data shown in Fig. 5). The decrease and broadening of the transmission null are due to an increase in scattering associated with the cantilever beam array.

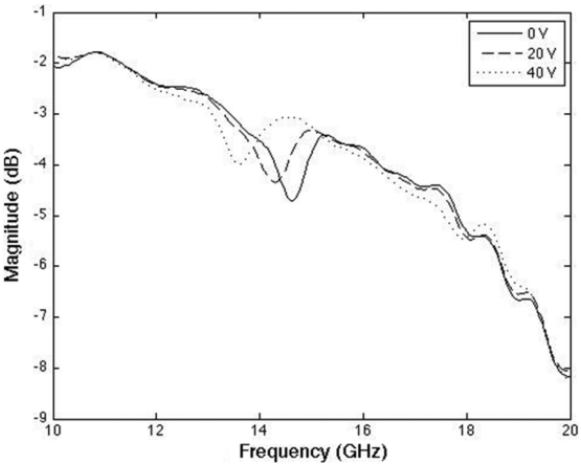

Fig. 8. Transmission from a 1 × 17 array of the cantilever embedded SRR structures. As the applied voltage is increased from 0 to 40 V, the resonant frequency shifts from 14.65 to 13.65 GHz.

The resonance did not shift until the applied voltage reached 20 V, corresponding to the actuation of the first cantilever beam. The cantilever pulls in, and the resonant frequency discretely shifts to 14.3 GHz, which is a shift of 0.35 GHz. With four beams raised and one beam pulled in, the estimated added

capacitance is 2.2 pF. At 40 V, the resonance again discretely shifts to 13.65 GHz indicating that more of the cantilevers have been actuated (i.e., reached their individual pull-in voltage). Given the variation in the pull-in voltage measurements due to the leakage current in the modified (FIB cut) SRR, it is possible that both the second and third cantilevers actuate in some of the SRR array elements at 40 V. Only 2-V steps were observed before the increased applied voltage caused the PECVD-grown nitride layer, in the beam contact region, to break down and make the device inoperable.

An overall shift in the measured resonant frequency of 1 GHz was observed. The observed frequency shift is approximately ten times larger than that predicted from the simulation models. This discrepancy could be a result of fringing fields that contribute to the capacitance of the devices but whose effects were neglected in the capacitance calculations used for the CST MWS simulation models.

The tunable SRR devices exhibit a single resonance at 14.65 GHz that has an initial transmission of 4.75 dB that decreases as the cantilevers are actuated. With 20 V applied, the transmission drops to 4.5 dB, and with 40 Vdc, the transmission is 4.0 dB. The observed loss in transmission magnitude is due to an increase in scattering of the incident radiation from the addition of the cantilevers to the SRRs.

SECTION VI. Conclusion

Tunable SRRs have been successfully fabricated with *in situ* MEMS cantilever beam arrays integrated into the gap region to electrostatically vary the resonant frequency. The cantilever beams actuated at low voltages one at a time. The inclusion of a FIB cut in the design not only stopped the dc voltage line from shorting to the outer SRR but also caused the device to operate at higher voltages leading to the eventual breakdown of the PECVD nitride layer. Despite the limited functionality, RF strip line measurements confirm that changes in capacitance due to the electrostatic actuation of the cantilevers are capable of tuning SRR resonant frequencies. The frequency was successfully tuned from 14.65 to 13.65 GHz as the cantilever beams were actuated. Additionally, this novel approach to meta-atom tuning is scalable to other resonant frequencies since the SRRs and the MEMS tuning elements are fabricated at the same time.

ACKNOWLEDGMENT

The authors would like to thank R. Johnston and R. Patton for their cleanroom support and assistance in depositing thin films.

The views expressed in this paper are those of the authors and do not reflect the official policy or position of the U.S. Air Force, Department of Defense, or the U.S. Government.

References

1. R. Marqus, F. Martn, M. Sorolla, Metamaterials With Negative Parameters, NJ, Hoboken:Wiley, pp. 52-54, 2008.

2. J. B. Pendry, A. J. Holden, D. J. Robbins, W. J. Stewart, "Magnetism from conductors and enhanced non linear phenomena", *IEEE Trans. Microw. Theory Tech.*, vol. 47, no. 11, pp. 2075-2084, Nov. 1999.

3. I. Gil, F. Martin, X. Rottenberg, W. De Raedt, "Tunable stop-band filter at Q-band based on RF-MEMS metamaterials", *Electron. Lett.*, vol. 43, no. 21, pp. 1153, Oct. 2007.

4. O. Reynet, O. Acher, "Voltage controlled metamaterial", *App. Phys. Lett.*, vol. 84, no. 7, pp. 1198-1200, Feb. 2004.

5. E. Ekmekci, K. Topalli, T. Akin, G. Turhan-Sayan, "A tunable multi-band metamaterial design using micro-split SRR structures", *Opt. Exp.*, vol. 17, no. 18, pp. 16046-16058, Aug. 2009.

6. S. Lim, C. Caloz, T. Itoh, "Metamaterial-based electronically controlled transmission line structure as a novel leaky-wave antenna with tunable radiation angle and beamwidth", *IEEE Trans. Microw. Theory Tech.*, vol. 53, no. 1, pp. 161-173, Jan. 2005.

7. S. Xiao, U. Chettiar, A. Klidshev, V. Drachev, I. C. Khoo, V. Shalaev, "Tunable magnetic response of metamaterials", *App. Phys. Lett.*, vol. 95, no. 3, pp. 033115-1-033115-3, July 2009.

8. T. Hand, S. Cummer, "Characterization of tunable metamaterial elements using MEMS switches", *IEEE Antennas Wireless Propag. Lett.*, vol. 6, pp. 401-404, 2007.

9. M. Sterner, D. Chicherin, A. V. Raisenen, G. Stemme, J. Oberhammer, "RF MEMS high-impedance tunable metamaterials for millimeter-wave beam steering", *Proc. IEEE 22nd Int. Conf. MEMS*, pp. 896-899, 2009-Jan.

10. D. Smith, D. C. Vier, T. Koschny, C. M. Soukoulis, "Electromagnetic parameter retrieval from inhomogeneous metamaterials", *Phys. Rev. E*, vol. 71, no. 3, pp. 036617, Mar. 2005.

11. 2010.

12. J. K. Luo, M. Lin, Y. Q. Fu, L. Wang, A. J. Flewitt, S. M. Spearing, N. A. Fleck, W. I. Milne, "MEMS based digital variable capacitors with a high-\$k\$ dielectric insulator", *Sens. Actuators A Phys.*, vol. 132, no. 1, pp. 139-146, May 2006.